

Long-lifetime, potentially low-cost anthraquinone flow battery chemistry developed from study of effects of water-solubilizing group and connection to core

Yan Jing¹, Eric M. Fell², Min Wu², Shijian Jin², Yunlong Ji^{1,4}, Daniel A. Pollack³, Zhijiang Tang², Dian Ding¹, Meisam Bahari,² Marc-Antoni Goulet,^{2,5} Tatsuhiko Tsukamoto¹, Roy G. Gordon^{1,2}✉, Michael J. Aziz²✉

¹Department of Chemistry and Chemical Biology, Harvard University, Cambridge, Massachusetts 02138, USA.

²John A. Paulson School of Engineering and Applied Sciences, Harvard University, Cambridge, Massachusetts 02138, USA.

³Department of Physics, Harvard University, Cambridge, Massachusetts 02138, USA.

⁴Present address: School of Chemistry and Materials Science, Hangzhou Institute for Advanced Study, University of Chinese Academy of Sciences, 1 Sub-lane Xiangshan, Hangzhou 310024, China.

⁵Present address: Department of Chemical and Materials Engineering, Concordia University, Montreal, Quebec, Canada.

✉e-mail: gordon@chemistry.harvard.edu; maziz@harvard.edu.

Abstract

Water-soluble anthraquinones (AQs) hold great promise serving as redox-active species in aqueous organic redox flow batteries. Systematic investigations into how the properties of redox molecules depend on the water-solubilizing groups and the way in which they are bound to the redox core are, however, still lacking. We introduce water-solubilizing groups linked to anthraquinone by C=C bonds via Heck cross-coupling reactions and convert C=C bonds to C–C bonds through hydrogenation. The anthraquinone and the ending groups are connected via branched or straight chains with either unsaturated or saturated bonds. We investigate the influence of water-solubilizing chains and ionic ending groups on redox potentials of molecules and identify three important trends. (1): The electron-withdrawing ending groups can affect redox potentials of AQs with two unsaturated hydrocarbons on the chains through π -conjugation. (2): For chains with two saturated or unsaturated straight hydrocarbons, water-solubilizing ending groups increase redox potentials of the AQs in the order of $\text{PO}_3^{2-} < \text{CO}_2^- < \text{SO}_3^-$. (3): AQs with saturated and unbranched chains at high pH possess desirably low redox potentials, high solubilities, and high stability. Disproportionation leads to the formation of anthrone, which can be regenerated to anthraquinone. Tautomerization results in the saturation of alkene chains, stabilizing the structure. We utilize these

observations to identify a potentially low-cost and long-lifetime negolyte that demonstrates a temporal fade rate as low as 0.0128%/day when paired with a potassium ferrocyanide posolyte.

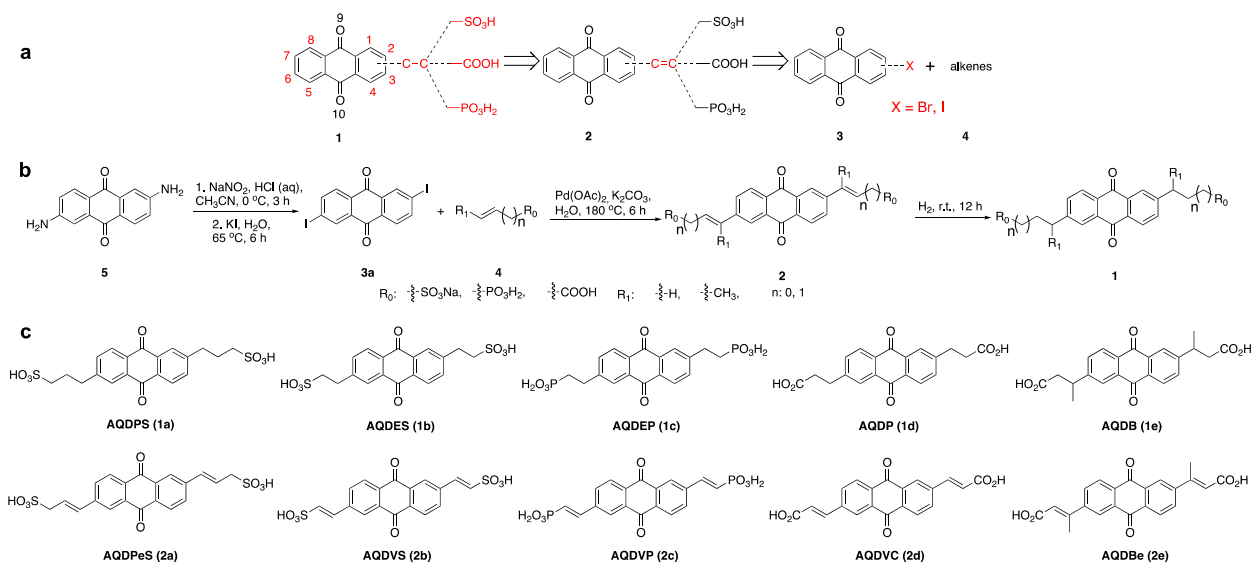
Introduction

Energy storage systems have become an integral part of modern society.^{1, 2} Among the most promising electricity storage systems are aqueous redox flow batteries (ARFBs). Featuring intrinsically nonflammable electrolytes, and decoupled energy and power scaling, ARFBs can play a crucial role in storing massive amounts of electricity produced from intermittent renewable resources such as solar energy and wind power and releasing the electricity when it is needed. Among a variety of ARFBs, the vanadium redox flow battery (VRFB) has been the most developed and mature system to-date.^{3, 4} Redox-active organic molecules composed of earth-abundant elements such as carbon, hydrogen, oxygen, nitrogen, and sulfur are potentially cost-effective.^{5, 6} Furthermore, because of structural diversity and tunability of organic molecules, molecular engineering can be employed to judiciously design desired redox molecules for aqueous organic redox flow batteries (AORFBs).^{7, 8} Although extremely stable anthraquinone-based aqueous flow batteries have been developed with projected decadal lifetime,⁹ manufacturing costs remain challenging. Additionally, the technology still stands to benefit greatly from improved synthetic methods, as well as systematic investigations into how the properties of redox molecules depend on the water-solubilizing groups and the way in which they are bound to redox cores.

Water-soluble quinone derivatives used for AORFBs comprise two motifs, the hydrophobic quinone redox center and the hydrophilic water-solubilizing groups, including $-\text{SO}_3^-$,⁶ $-\text{CO}_2^-$,¹⁰ $-\text{PO}_3^{2-}$,¹¹ $-\text{NR}_4^+$,¹² $^{13} \text{O}^-$,⁷ and polyethylene glycol (PEG)¹⁴. These motifs are connected via covalent bonds such as C–O,¹⁴ C–S,¹⁵ and C–C⁹ or are directly attached to redox cores.^{6, 7, 16, 17} It appears that redox cores bonded to water-solubilizing groups via C–heteroatom bonds are susceptible to nucleophilic substitution reactions, resulting in the detachment of water-solubilizing groups from redox cores.^{10, 18, 19} Because carbon-carbon bonds are more chemically resistant against nucleophilic attack than carbon-heteroatom bonds such as C–O (S, N), it is desirable to incorporate carbon-carbon bonds between redox centers and water-solubilizing ending

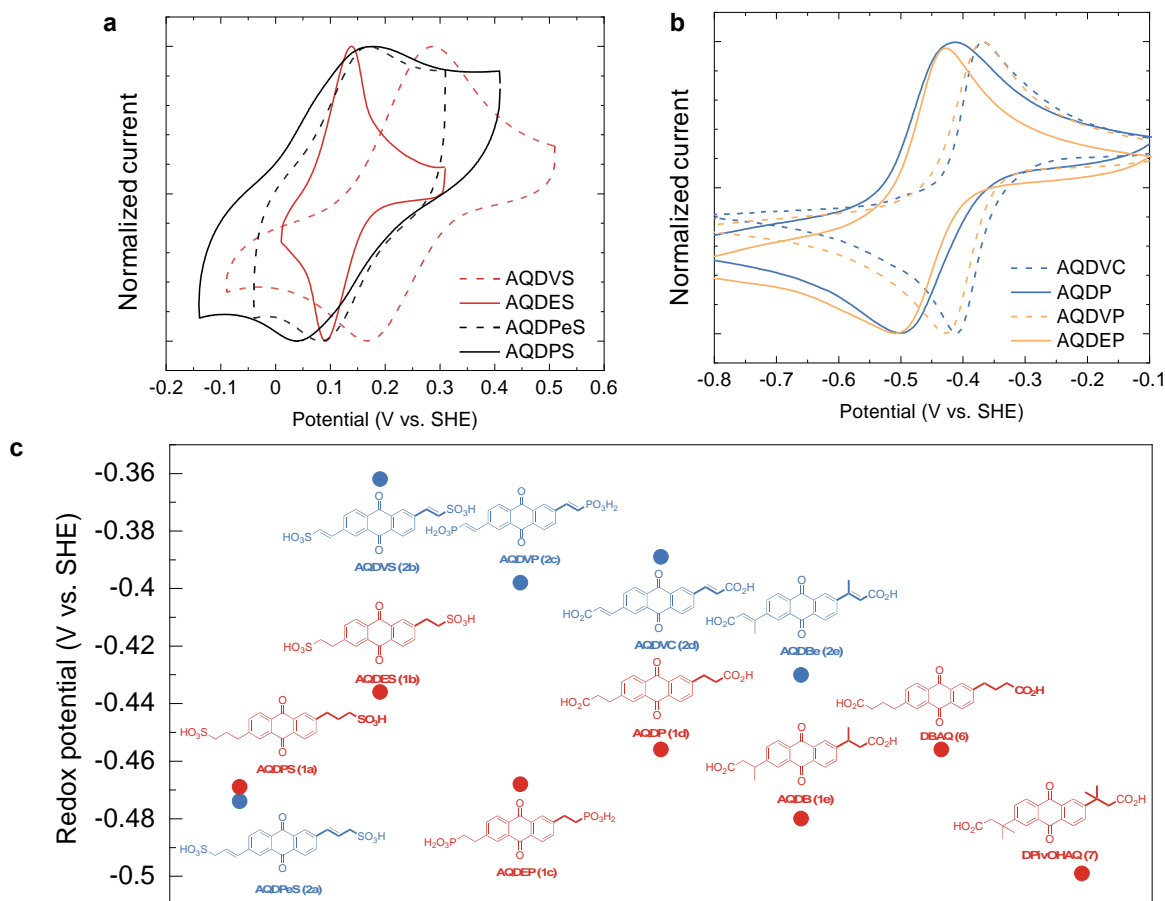
groups.⁹ Redox centers and $-\text{SO}_3^-$, $-\text{CO}_2^-$, $-\text{PO}_3^{2-}$ water-solubilizing groups are considered electron-withdrawing because of their resonance and negative inductive effects. When there is only a single unsubstituted methylene group ($-\text{CH}_2-$) between a redox center and a water-solubilizing group, the close proximity of the electron-withdrawing groups to the redox core may cause molecules to be vulnerable to nucleophilic attack.^{13, 20, 21} In contrast, excellent molecular stability has been achieved when there are at least two carbon atoms between water-solubilizing groups and redox cores.^{9, 13}

Here we demonstrate a generic method for synthesizing water-soluble anthraquinone (AQ) derivatives with saturated or unsaturated and branched or straight carbon linkages (Scheme 1). Specifically, 2,6-diamino-9,10-anthraquinone is transformed to 2,6-diiodo-9,10-anthraquinone. Then, C=C linked water-solubilizing groups are introduced via Heck cross-coupling reactions to afford water-soluble anthraquinones with unsaturated carbon linkages. Hydrogenation of these molecules then converts C=C bonds to C–C bonds. Using the same synthetic method, we synthesized ten anthraquinone derivatives, each with one of three water-soluble ending groups ($-\text{SO}_3^-$, $-\text{CO}_2^-$, $-\text{PO}_3^{2-}$) and a particular (branched/straight, unsaturated/saturated) carbon linkage. We evaluated their solubility, stability, redox potentials, standard rate constants, and diffusion coefficients to better understand the effects of different solubilizing groups and linkages. In the end, we identified 9,10-anthraquinone-2,6-dipropionic acid (**AQDP**) as an extremely stable and potentially low-cost negative electrolyte (negolyte). When paired with potassium ferrocyanide positive electrolyte (posolyte), **AQDP** exhibits a temporal fade rate as low as 0.012% per day.



Scheme 1 | (a) Retrosynthetic analysis of $-C_2H_4-$ linked water-soluble anthraquinones (AQs). (b) The synthetic routes and conditions used for the synthesis of a class of water-soluble AQs. (c) Water-soluble anthraquinones synthesized by the same method.

Following the reasoning that a stable redox molecule should have at least two carbons between a redox core and a water-solubilizing group, we consider Heck cross-coupling to be a plausible route to access the desired water-soluble anthraquinones (**1** and **2**). Specifically, halogenated anthraquinones (**3**) can react with easily accessible water-soluble alkenes (**4**) to afford anthraquinones bearing water-solubilizing groups separated from the anthraquinone core by at least two carbons, and the tethered alkenyl chains can be saturated via hydrogenation (**Scheme 1**). We selected a variety of alkenes (**4**) containing SO_3^- , CO_2^- , and PO_3^{2-} ending groups to react with **3**. First, 2,6-diaminoanthraquinone (**5**) is converted to 2,6-diiodoanthraquinone (**3a**) through the intermediate diazotization (**Scheme 1b**). Then **3a** was subjected to palladium-catalyzed Heck cross-coupling reactions using different water-solubilizing coupling partners to afford **2a-2e**. After the completion of the Heck reaction, hydrogen gas was introduced in the reaction to afford **1a-1e** through a one-pot Heck reaction–hydrogenation sequence. **Scheme 1c** lists all carbon-linked AQs synthesized by this method. Both unsaturated and saturated as well as branched and straight hydrocarbon chains were introduced; the number of carbon atoms on each chain is 2–4.



Carbon linked water-soluble anthraquinones

Fig. 1 | Cyclic voltammograms (CVs) on glassy carbon and redox potentials of the water-soluble AQs. (a): CVs of **AQDVS**, **AQDES**, **AQDPeS**, and **AQDPS** in 1 M H₂SO₄; (b) CVs of **AQDVC**, **AQDP**, **AQDVP**, **AQDEP** in 1 M KOH. Scan rate: 100 mV/s. Concentration of AQs: 5 mM. (c) Mapping the redox potentials of 12 water-soluble anthraquinones at pH 14, including two previously reported carbon-linked AQs, DPivOHAQ: 3,3'-(9,10-anthraquinone-diyl)bis(3-methylbutanoic acid); DBAQ: 4,4'-(9,10-anthraquinone-diyl)dibutanoic acid.^{9, 22} The AQs with saturated chains are red colored, and the AQs with unsaturated chains are blue colored. All CV measurements were collected at room temperature with a scan rate of 100 mV/s.

Fig. 1 shows the cyclic voltammogram (CV) results of AQs at pH 0 and 14 and a map of redox potentials at pH 14. For those AQs with two unsaturated hydrocarbons on the chains, the electron-withdrawing ending groups (SO₃⁻, PO₃²⁻, COO⁻) can still affect the redox potentials through π -conjugation. Consequently, the redox potentials of **AQDVS** (2b), **AQDVP** (2c), **AQDVC** (2d) are 60–80 mV higher than those of the saturated AQs, *i.e.*, **AQDES** (1a), **AQDEP** (1c), **AQDP** (1d), where the negative resonance effect is

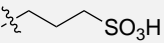
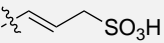
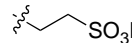
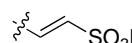
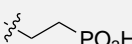
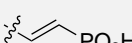
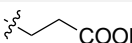
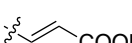
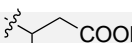
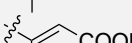
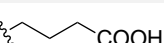
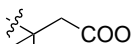
weakened due to the saturated hydrocarbon linkage. We also noticed that those molecules show a clear trend in redox potentials, *i.e.*, **2b** > **2d** > **2c** for the unsaturated AQs and **1b** > **1d** > **1c** for the saturated AQs (Fig. 1c), which is supported by the theoretical calculation of water-solubilizing groups increasing redox potentials in the order of $\text{SO}_3^- > \text{CO}_2^- > \text{PO}_3^{2-}$.²³

Interestingly, **AQDPeS (2a)** has a slightly lower redox potential than its saturated analogue **AQDPS (1a)**. This effect may be explained by the two unsaturated C=C bonds extending the conjugation of the anthraquinone core and enhancing the resonance effect in **2a**; meanwhile, the saturated methylene group may weaken the negative resonance effect of SO_3^- . The same trend is also found at pH 0; the potential of **1b** (110 mV vs. SHE) is 115 mV lower than that of **2b** (225 mV vs. SHE); whereas the potential of **1a** (122 mV vs. SHE) is slightly higher than that of **2a** (98 mV vs. SHE) (Fig. 1a).

The effect of branched alkyl chains on redox potentials can be evaluated through the comparison of **1d**, **AQDB (1e)**, and **DPivOHAQ (7)**.⁹ Addition of electron-donating methyl groups on the benzylic carbons can lead to lower redox potentials of AQs, with the order of potentials given by **7** (−0.499 V) < **1e** (−0.480 V) < **1d** (−0.456 V). A similar trend is also found from the unsaturated AQs, *i.e.*, **2e** (−0.430 V) < **2d** (−0.389 V).

For those AQs possessing saturated and straight chains with different numbers of carbon atoms, the redox potential of **1a** (−0.469 V) is 33 mV lower than that of **1b** (−0.436 V), whereas the redox potential of **1d** (−0.456 V) is the same as that of **DBAQ (6)** (−0.456 V) (Fig. 1c). The difference suggests that the inductive electron-withdrawing effect of CO_2^- can be sufficiently weakened by two saturated carbons, whereas SO_3^- still plays a role in elevating redox potential even when distanced by two saturated carbons.

135 Table 1 | Properties of carbon-linked water-soluble AQs. The pH was adjusted by KOH.

| Molecule | Number | Chains | Redox potential @ pH 14 (V) | Peak separation (mV) | Solubility (M) |
|-----------------|-----------|--|--------------------------------|-------------------------|----------------------------|
| AQDPS | 1a |  | -0.469 | 50 | 0.30 @ pH 7 |
| AQDPeS | 2a |  | -0.474 | 138 | 0.35 @ pH 7 |
| AQDES | 1b |  | -0.436 | 53 | 1.10 @ pH 0 0.30 @ pH 7 |
| AQDVS | 2b |  | -0.362 | 63 | 0.10 @ pH 0 |
| AQDEP | 1c |  | -0.468 | 80 | 1.10 @ pH 12 |
| AQDVP | 2c |  | -0.398 | 56 | 0.85 @ pH 12 |
| AQDP | 1d |  | -0.456 | 83 | 1.00 @ pH 12 |
| AQDVC | 2d |  | -0.389 | 42 | 0.70 @ pH 12 |
| AQDB | 1e |  | -0.480 | 98 | 0.77 @ pH 12 |
| AQDBe | 2e |  | -0.430 | 86 | 0.65 @ pH 12 |
| DBAQ | 6 |  | -0.456 | 83 | 1.00 @ pH 12 |
| DPivOHAQ | 7 |  | -0.499 | 52 | 0.75 @ pH 12 |

136

137 The aqueous solubility of AQs depends on solution pH, ending groups, and the chains with (un)saturated,

138 (un)branched hydrocarbons between the redox cores and ending groups. The solubilities of these AQs are

139 summarized in Table 1. The solubility of **1b** reaches 1.10 M at pH 0 due to the negative pK_a of $-\text{SO}_3\text{H}$,

140 whereas its solubility decreases to 0.30 M when pH is adjusted to 7 by adding KOH. Similarly, the solubility

141 of anthraquinone-2,7-disulfonic acid (AQDS) is 1.50 M at pH 0,⁶ and its solubility decreases to 0.58 M at

142 pH 7 when the pH is adjusted by adding NaOH.²⁴ At pH 12, $-\text{CO}_2\text{H}$ and $-\text{PO}_3\text{H}_2$ are fully deprotonated,

143 and the solubilities of **1c**, **1d**, and **6** at pH 12 reach 1.1 M, 1.0 M, 1.0 M, respectively. AQs with unsaturated

144 chains usually show lower solubilities than their saturated versions, *i.e.*, **1b** > **2b**; **1c** > **2c**, **1d** > **2d**. A

145 plausible explanation is that the extended conjugation in the unsaturated AQs enhances the intermolecular

146 π - π interactions, thus lowering their solubility in water. In addition, the solubility of AQs tends to decrease

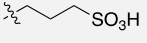
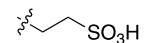
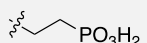
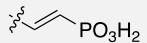
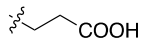
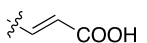
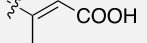
147 when more hydrophobic hydrocarbons are incorporated to chains. For example, the solubility of **2e** is lower

148 than that of **2c** as one extra branched methyl group is introduced in **2e**. Similarly, the solubility of **6** is

slightly lower than that of **1d** as there are three methylene groups between the AQ and ending groups in **6** and two in **1d**.

Table 2 | Properties of carbon-linked water-soluble AQs. (cont.)

All molecules were prepared with a concentration of 5 mM and tested at pH 14.

| Molecule | Number | Chains | Diffusion coefficient (cm ² /s) | | k _o (cm/s) | | α from RDE |
|--------------|-----------|--|--|----------|-----------------------|----------|------------|
| | | | from CV (underestimate) | from RDE | from CV (simulate) | from RDE | |
| AQDPS | 1a |  | 5.6e-7 | 9.8e-7 | 4.5e-3 | 3.0e-3 | 0.74 |
| AQDES | 1b |  | 4.3e-8 | 1.3e-7 | 1.5e-3 | 4.0e-3 | 0.50 |
| AQDEP | 1c |  | 2.5e-7 | 8.6e-7 | 1.5e-3 | 1.4e-3 | 0.72 |
| AQDVP | 2c |  | 6.5e-7 | 1.1e-6 | 6.5e-3 | 2.2e-3 | 0.65 |
| AQDP | 1d |  | 1.8e-7 | 9.5e-7 | 1.6e-3 | 3.4e-3 | 0.72 |
| AQDVC | 2d |  | 6.2e-7 | 1.1e-6 | 5.3e-3 | 3.3e-3 | 0.61 |
| AQDBe | 2e |  | 2.8e-8 | 3.8e-7 | 1.9e-3 | 5.5e-3 | 0.66 |

The electrochemical kinetics of seven AQs were investigated; in particular, their rate constants and diffusion coefficients were extracted from cyclic voltammetry and rotating disc electrode experiments (Figure S16-30, Supporting Information). CVs were evaluated at multiple scan rates in pH 14 supporting electrolyte, with all molecules investigated demonstrating quasi-reversible, two-electron redox processes. Using the Randles-Ševčík equation, a plot of voltammogram peak currents vs. the square root of scan rate provides a slope from which a diffusion coefficient can be calculated. However, it must be noted that by using the Randles-Ševčík equation, the diffusion coefficient will be underestimated whenever the observed redox process is not fully reversible, as is always the case in this study. Therefore, linear sweep voltammetry with a rotating disk electrode was used to determine more accurate values for diffusion coefficients. Using these diffusion coefficients, CVs were then fit by simulation²⁵ to the experimental data to determine electrochemical rate constants of the limiting reduction process (*k_o*) and formal reduction potentials of the individual electron redox processes (*E⁰₁*, *E⁰₂*). Rate constants determined from CV simulation and RDE

were both in good agreement with each other (see **Table 2**). As others have noted, *ex situ* electrochemical characterization of ARFB active species is almost always performed on flat macroelectrodes (e.g. glassy carbon), yet these molecules are then tested in flow batteries with porous carbon electrodes of varied surface composition where electron transfer kinetics quantification is further complicated by mass transport.^{26 27, 28} Thus the electrochemical kinetics of these AQs may differ when porous carbon electrodes are used in a flow battery, possibly even resulting in slower electrochemical kinetics.^{29, 30}

The structure-property relationships between AQs and their redox potentials and solubilities have been evaluated in detail; all the tested AQs show similar standard rate constants and diffusion coefficients. Plausible explanations for the similar rate constants are: AQ cores dominate and the chains are not bulky enough to provide steric hindrance; the linking manners and water-solubilizing groups appear not to affect the rate constants; the extension of the π system in the unsaturated AQs over the saturated ones does not affect the rate constants of AQs. Additionally, it is unlikely that a significant difference in standard rate constants would be observed given that minimal solvation reorganization upon reduction/oxidation, typical for AQs, allows for fast electrochemical kinetics.³¹

All AQs show similar diffusion coefficients because all the AQ molecules have very similar molecular sizes.

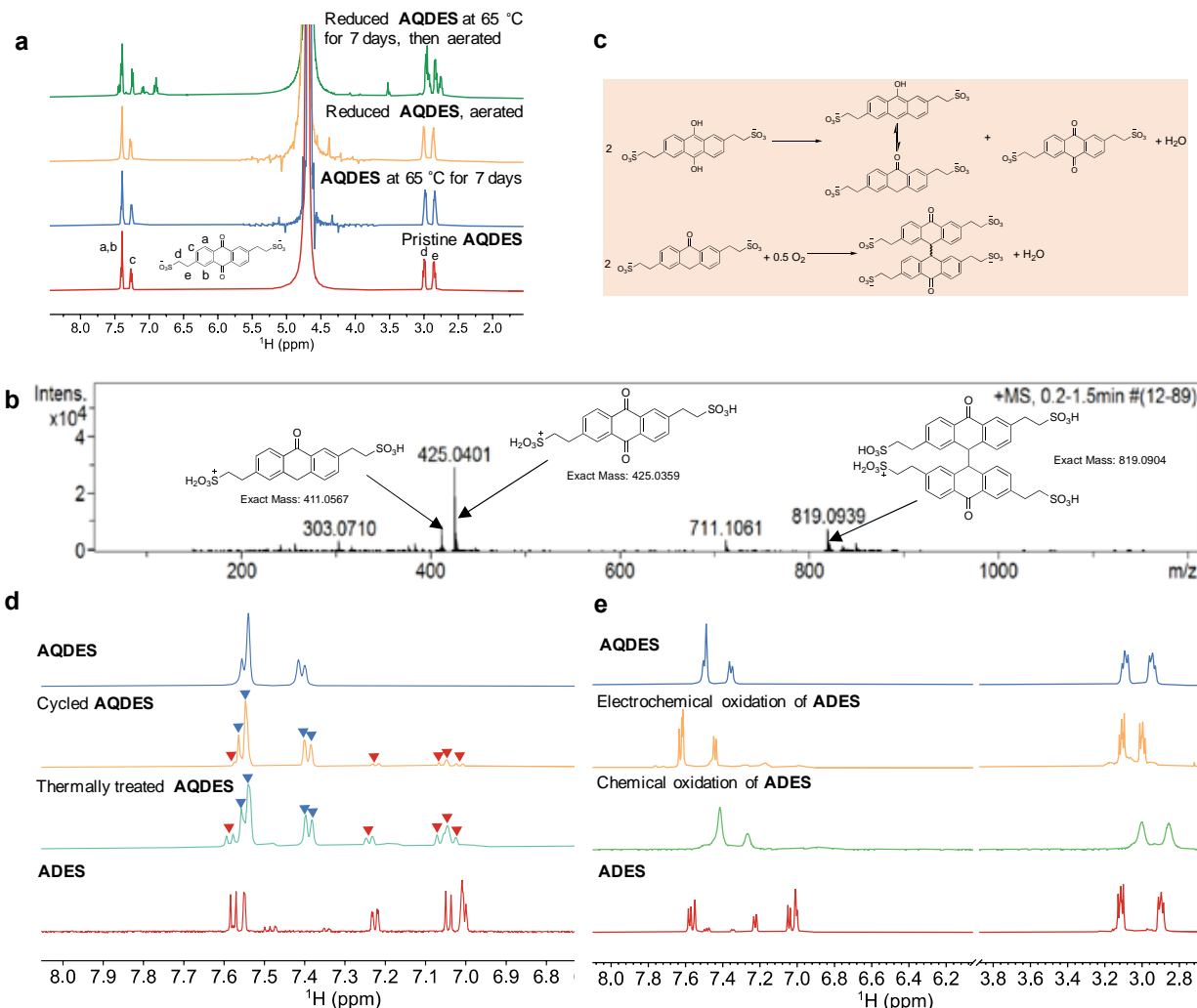


Fig. 2 | Structural stability studies of **1b and its reduction product in 1 M H₂SO₄.** (a) Thermal stability as evaluated by ¹H NMR spectroscopy. **1b** is thermally stable at elevated temperatures (65 °C) over 7 days, whereas the reduction product of **1b** is thermally unstable, as indicated by the decomposition peaks. The signal at 4.79 ppm is from the solvent (water). (b) Mass spectrum suggests the formation of anthrone and anthrone dimer derivatives. Positively ionized (protonated), m/z = exact mass of protonated molecules with one positive charge. (c) Proposed decomposition pathways in which the decomposition compounds were detected by mass spectrometry. (d) Stacked ¹H NMR of (from top to bottom) pristine, cycled, thermally treated (reduction product treated at 65 °C for 7 days, then aerated) AQDES and chemically synthesized diethylsulfonated-2,6-anthrone (anthranol) (ADES), suggesting that the decomposition compound in the cycled and thermally treated AQDES is ADES. (e) Stacked ¹H NMR of (from top to bottom) pristine AQDES, electrochemically oxidized AQDES from ADES, chemically oxidized AQDES from ADES by CrO₃ in acidic conditions, and ADES, suggesting that ADES can be (electro)chemically oxidized to AQDES.

Commercially viable batteries for grid storage are expected to have operating lifetimes exceeding 10 years.³² Chief among the degradation mechanisms that limit the lifetime of organic flow batteries is the molecular decomposition of the organic species themselves. In addition to cost and resource limitations,

technical challenges restrict the length of cycling experiments at the lab scale to assess the intrinsic stability of these reactants. Accelerating these decomposition mechanisms through higher temperature experiments is the most direct way to accelerate research and development of new viable compounds.^{33, 34}

The stability of redox molecules is of utmost importance because it determines whether the molecule is eventually useful for real applications. It is thus necessary to independently evaluate the stability of a redox molecule before running a full cell in which counter electrolytes, membrane, and electrodes will be involved and complicate the analysis. A protocol that has proven to be effective is to store electrolytes with different states of charge (SOC) at reasonably elevated temperatures and operational pH, which can accelerate molecular decompositions of both states. Depending on decomposition rates, decomposition compounds can be detected by liquid chromatography–mass spectroscopy (LC–MS) or ¹H NMR spectroscopy.^{9-11, 35}

Given that the redox potential of **1b** is 110 mV vs. RHE at pH 0 and the solubility of **1b** is 1.1 M, it is worthwhile to investigate its thermal stability in acid for both redox states. The ¹H NMR spectra in **Fig. 2a** suggests that **1b** is thermally stable, whereas the reduction product of **1b** is not. The sample showing ¹H NMR decomposition peaks in **Fig. 2a** was further analyzed by mass spectrometry. The characteristic *m/z* values (**Fig. 2c**) suggest decomposition of the reduction product of **1b**; its anthrone and anthrone dimer derivatives were produced over 7 days at 65 °C. These decomposition compounds have been observed in previous studies supported by theoretical calculations.³⁶ To further confirm the formation of anthrone derivatives, we chemically synthesized diethylsulfonated-2,6-anthrone (anthranol) (ADES),³⁶ and found that its ¹H NMR chemical shifts and peak splitting are indeed in line with those in the cycled and thermally treated AQDES spectra (**Fig. 2d**). We previously found that anthrone derivatives can be chemically oxidized to AQs when exposed to air or other oxidants^{9, 36, 37} and electrochemically oxidized back to AQs when proper potentials are applied.³⁷ We built an electrochemical cell of 5 mL, 0.05 M ADES paired with 15 mL, 0.1 M AQDS (anthraquinone-2,7-disulfonate) in 1 M H₂SO₄ for ADES electrochemical oxidation. A constant current of 2 mA/cm² was applied until the potential of ADES vs. AQDS reached 1.7 V. After that, an aliquot of ADES solution was taken and diluted with D₂O for ¹H NMR measurement. Our

preliminary (electro)chemical oxidation results confirmed the conversion of ADES to AQDES (**Fig. 2e**), suggesting that it would be plausible to *in situ* electrochemically regenerate redox-active AQDES from redox-inactive ADES in flow batteries.

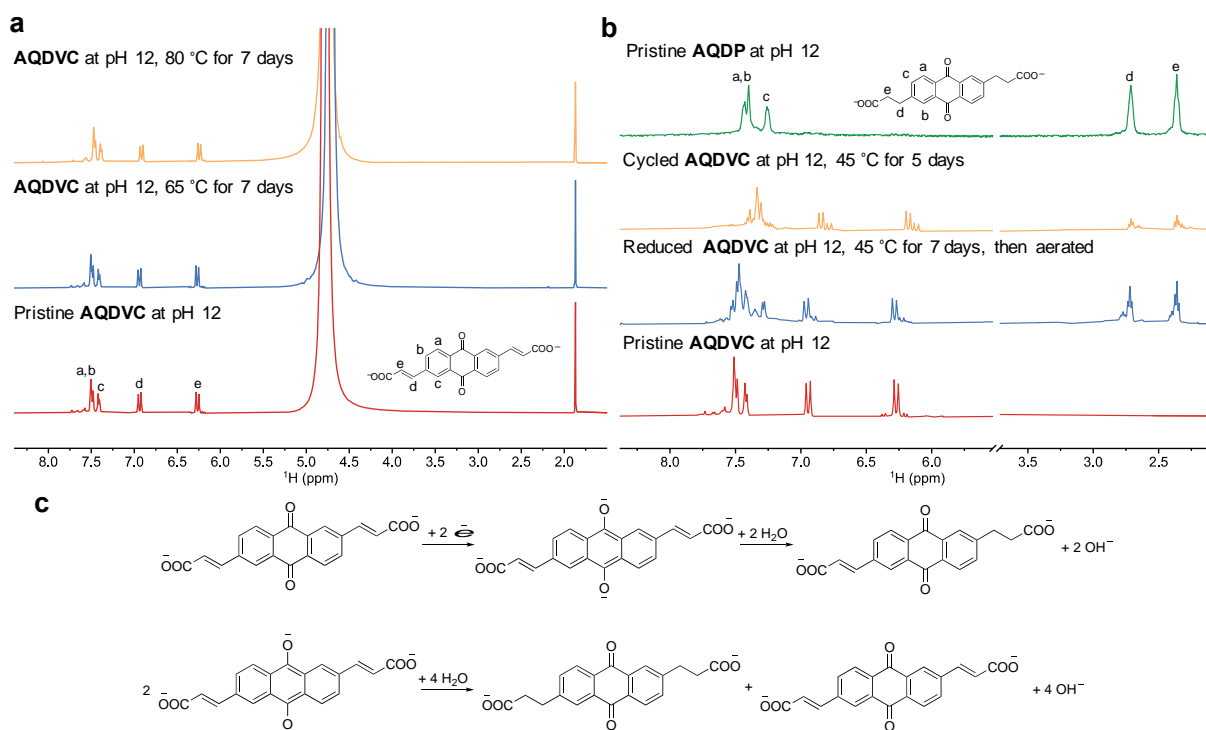


Fig. 3 | Structural stability studies of **2d** and its reduction product at pH 12. Thermal stability was measured by ^1H NMR spectroscopy. (a) **2d** at pH 12 is thermally stable at elevated temperatures (65 °C) over 7 days. The signal at 1.85 ppm is from the internal standard (potassium acetate), and the signal at 4.79 ppm is from the solvent (water). (b) The reduction product **2d** at pH 12 is thermally unstable at 45 °C after 7 days, which is indicated by the appearance of new peaks in both aromatic and aliphatic regions. The chemical shifts of the new peaks are either similar or identical to those of **1d**, suggesting that the reduction product of **2d** may tautomerize to molecules similar to **1d**. (c) Decomposition compounds were detected by LC–MS and proposed possible decomposition pathways are illustrated (see Supporting Information).

To achieve commercial viability, AORFB electrolytes must be extremely stable and also have a lower capital cost than existing vanadium flow battery electrolytes. Among the AQs reported in the present work, **1d** and **2d** are synthesized from anthraquinone precursor and acrylic acid, the latter being a major building block in the production of many industrial products. Therefore, **1d** and **2d** could be potentially low-cost once the synthetic conditions are fully optimized. The evaluation of the stability of **2d** in both oxidation states at pH 12 is presented in **Fig. 3**. Although the unchanged spectra in **Fig. 3a** indicate that **2d** is stable at both 65 °C and 80 °C after 7 days, the new peaks appearing in both aromatic and aliphatic regions in **Fig.**

3b suggest that the reduction product of **2d** is unstable when stored at 45 °C for 7 days. Interestingly, the chemical shifts of the new peaks are either similar or identical to those of **1d**. The m/z ratio obtained from LC–MS experiments suggested the existence of **1d**, **2d**, and a compound with a molecular weight equal to 2 less than that of **1d** (or 2 more than that of **2d**), which we hypothesize is an intermediate possessing one saturated chain and one unsaturated chain. Corresponding reaction mechanisms are proposed in **Fig. 3c**. Tautomerization favors formation of the intermediate, and disproportionation leads to the formation of **1d** and **2d**.^{16, 38}

Given the instability of **2d**, we set out to evaluate the stability of saturated analogues. **1c** and **1d** are two molecules with two saturated hydrocarbon chains. Both redox states of each were stored at pH 14 and at 65 °C for 7 days and then characterized by ¹H NMR (**Fig. 4**). Identical spectra for the two molecules in both states indicate their excellent thermal stability. Through comparing redox potentials, solubility, rate constant, diffusion coefficient, and stability for all carbon-linked AQs, we notice that at high pH, water-soluble AQs with saturated chains demonstrate lower redox potentials, higher solubility, and better stability than their unsaturated versions; therefore, water-soluble AQs with saturated chains are desirable negolyte active species.

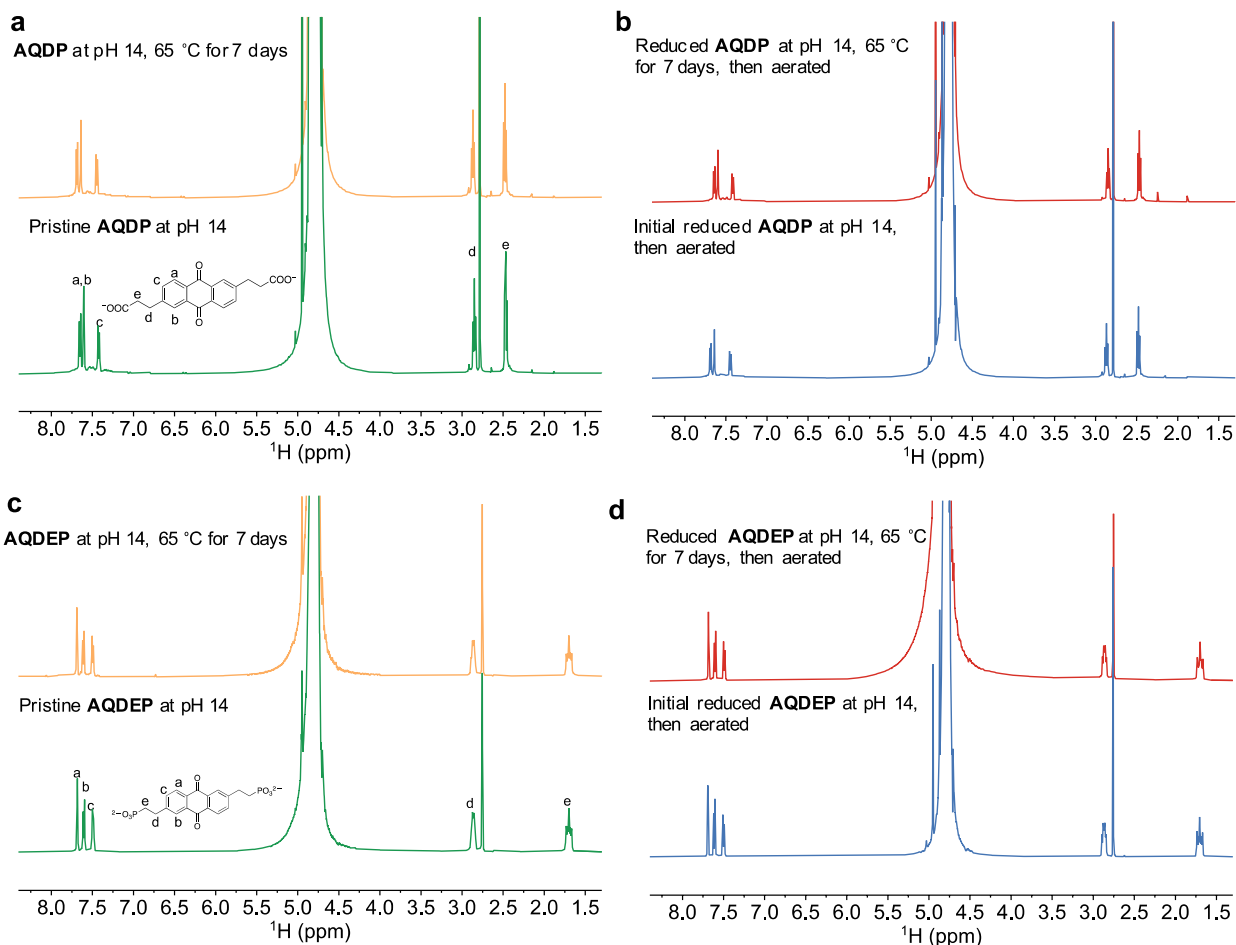


Fig. 4 | Structural stability studies of redox pairs **1c** and **1d** at pH 14. Thermal stability at elevated temperatures (65 °C) over 7 days was confirmed by ^1H NMR spectroscopy. (a) Stacked ^1H NMR spectra of **1d** at pH 14. (b) Stacked ^1H NMR spectra of the reduction product of **1d** at pH 14 after aeration. (c) Stacked ^1H NMR spectra of **1c** at pH 14. (d) Stacked ^1H NMR spectra of the reduction product of **1c** at pH 14 after aeration. The signal at 2.75 ppm is from the internal standard (sodium methanesulfonate). The signal at 4.79 ppm is from the solvent (water).

AQDP (1d) was chosen to be investigated in full cells given its potential low-cost in mass production, excellent stability, high solubility, and suitable redox potential. The voltage profile and the cell cycling in **Fig. 5a** and **5b** are from a 0.1 M **AQDP** full cell when paired with a potassium ferrocyanide polysolite. The full cell approached 94.5% of the theoretical capacity and exhibited a temporal fade rate of 0.0128% per day after being cycled for 8 days and 350 cycles, suggesting that **AQDP** is extremely stable.³⁴ The dip highlighted in **Fig. 5b** was caused by the temporary depletion of nitrogen, as the cell was cycled in a nitrogen-filled glove bag. A full cell with 1 M **AQDP** was built to demonstrate the feasibility of a concentrated flow cell operation. The concentrated cell exhibited a capacity utilization of 79.2% and a

temporal fade rate of 0.025% per day over 11 days. The lower capacity utilization and the fluctuations in capacity and Coulombic efficiency in **Fig. 5d** are possibly due to the concentration approaching the solubility limit and/or high mass transport resistance.^{10, 39} The fade rate of the concentrated cell (1 M **AQDP**) is approximately twice as high as that of the dilute cell (0.1 M **AQDP**), and further experimental investigation is required to examine whether the difference in fade rate is due to the difference in concentration.

Polarization curves at various SOC are shown in **Fig. 5e**. **AQDP** delivers a peak power density exceeding 180 mW/cm² at 90% SOC. The open circuit voltage of the full cell increases with increasing SOC and is approximately 0.98 V at 50% SOC. The high frequency resistance remains approximately 1.2 Ω cm² over the full SOC range (**Fig. 5f**), which is mainly due to the membrane resistance. The polarization resistance varies from 1.47 to 1.63 Ω cm², due to the nearly constant membrane resistance and the varying electrolyte resistance at different SOC.

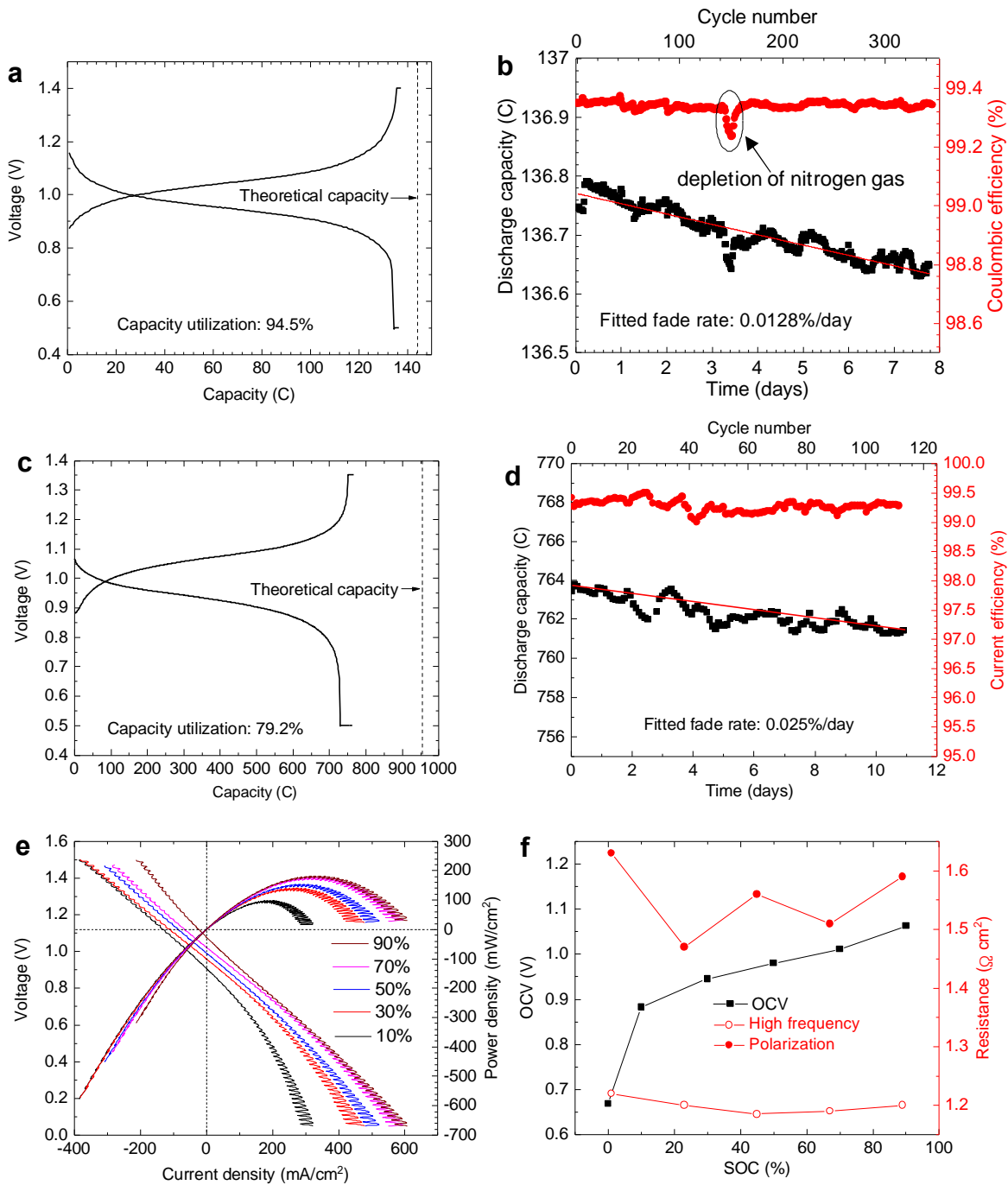


Fig. 5 | AQDP-based full cell measurements. (a, b): The voltage profile and long-term cycling of a 0.1 M AQDP-based full cell. Cell configuration: 7.5 mL, 0.1 M AQDP, 1 M KCl, pH 12 | 100 mL, 0.1 M $\text{K}_4\text{Fe}(\text{CN})_6$, 0.02 M $\text{K}_3\text{Fe}(\text{CN})_6$, 1 M KCl, pH 12. The cell was first charged/discharged at 30 mA/cm² until voltages reached 1.35 V or 0.5 V and then was held at these voltages until the current density dropped to 2 mA/cm². (c, d): The voltage profile and long-term cycling of a 1 M AQDP-based full cell. Cell configuration: 5 mL, 1 M AQDP, pH 12 | 100 mL, 0.5 M $\text{K}_4\text{Fe}(\text{CN})_6$, 0.1 M $\text{K}_3\text{Fe}(\text{CN})_6$, pH 12. The cell was first charged/discharged at 50 mA/cm² until voltages reached 1.35 V or 0.5 V and then was held at these voltages until the current density dropped to 2 mA/cm². (e) Cell voltage and power density versus

current density at room temperature at 10%, 30%, 50%, 70%, and 90% SOC. Oscillations in current density are due to the pulsations of the peristaltic pump. (f) OCV, as well as high frequency and polarization ASR versus SOC. For all tests, Fumesap® E620(K) was used as the membrane. The pH of electrolytes was adjusted by adding KOH pellets. Cell configuration for (e and f): 5 mL, 0.5 M **AQDP**, pH 12 | 100 mL, 0.5 M $\text{K}_4\text{Fe}(\text{CN})_6$, 0.1 M $\text{K}_3\text{Fe}(\text{CN})_6$, pH 12. The cell cycling tests were conducted in a N_2 -filled glove bag, and the polarization and ASR tests were conducted in a N_2 -filled glove box.

Conclusions

We designed and synthesized a class of carbon-linked water-soluble anthraquinones; compared redox potentials, rate constants, diffusion coefficients, and solubility of up to 12 quinones; and selectively evaluated thermal stability of four AQs. The trends that we observed are:

1. The electron-withdrawing ending groups (SO_3^- , PO_3^{2-} , CO_2^-) can affect redox potentials of AQs with two unsaturated hydrocarbons on the chains through π -conjugation, and the redox potentials of **AQDVS**, **AQDVP**, **AQDVC** are 60–80 mV higher than those of the saturated AQs, *i.e.*, **AQDES**, **AQDEP**, and **AQDP**.
2. In stark contrast, the redox potential of **AQDPeS** is lower than its saturated analogue **AQDPS** in both acidic and alkaline media. The two unsaturated $\text{C}=\text{C}$ bonds extend π conjugation of **AQDPeS** and the methylene groups next to the $\text{C}=\text{C}$ bonds in **AQDPeS** weaken the negative resonance effect of SO_3^- , thus lowering its potential.
3. For the AQs with two saturated or unsaturated straight hydrocarbons, water-solubilizing ending groups increase redox potentials of the AQs in the order of $\text{PO}_3^{2-} < \text{CO}_2^- < \text{SO}_3^-$, in agreement with theoretical predictions.
4. AQs with unsaturated chains show lower solubilities than their saturated counterparts.
5. The solubility of AQs decreases when more hydrophobic hydrocarbons are incorporated into chains.
6. AQs with saturated and unbranched chains at high pH possess desirably low redox potentials, high solubilities, and high stability.

We further detected anthrone and anthranol formation, along with possible saturation of unsaturated chains by tautomerization. The capacity fade caused by the formation of anthrone and anthranol, however, can be regenerated. We identified 9,10-anthraquinone-2,6-dipropionic acid as a negolyte candidate given

its potentially low-cost mass production and its demonstrated low temporal fade rate of 0.0128—0.025% per day when paired with a potassium ferrocyanide polysolite.

Conflicts of interest

Harvard University has filed a patent application on the materials described in the paper. M.J.A. has an ownership stake in Quino Energy, Inc., which might profit from these materials.

Acknowledgments

Research was supported by the U.S. National Science Foundation through grant CBET-1914543 and by U.S. DOE award DE-AC05-76RL01830 through PNNL subcontract 535264. D. A. P. acknowledges funding support from the NSF Graduate Research Fellowship Program, no. DGE1144152 and DGE1745303.

References

- Schmidt, O.; Hawkes, A.; Gambhir, A.; Staffell, I., The future cost of electrical energy storage based on experience rates. *Nature Energy* **2017**, 2 (8), 17110.
- Rugolo, J.; Aziz, M. J., Electricity storage for intermittent renewable sources. *Energy Environ. Sci.* **2012**, 5 (5), 7151–7160.
- Rychick, M.; Skyllas-Kazacos, M., Characteristics of a new all-vanadium redox flow battery. *J. Power Sources* **1988**, 22, 59–67.
- Roe, S.; Menictas, C.; Skyllas-Kazacos, M., A high energy density vanadium redox flow battery with 3 M vanadium electrolyte. *J. Electrochem. Soc.* **2016**, 163 (1), A5023–A5028.
- Narayan, S. R.; Nirmalchandrar, A.; Murali, A.; Yang, B.; Hoober-Burkhardt, L.; Krishnamoorthy, S.; Prakash, G. K. S., Next-generation aqueous flow battery chemistries. *Curr. Opin. Electrochem.* **2019**, 18, 72–80.
- Huskinson, B. T.; Marshak, M. P.; Suh, C.; Er, S.; Gerhardt, M. R.; Galvin, C. J.; Chen, X.; Aspuru-Guzik, A.; Gordon, R. G.; Aziz, M. J., A metal-free organic-inorganic aqueous flow battery. *Nature* **2014**, 505 (7482), 195–198.
- Lin, K.; Chen, Q.; Gerhardt, M. R.; Tong, L.; Kim, S. B.; Eisenach, L.; Valle, A. W.; Hardee, D.; Gordon, R. G.; Aziz, M. J.; Marshak, M. P., Alkaline quinone flow battery. *Science* **2015**, 349 (6255), 1529–1532.
- Xu, J.; Pang, S.; Wang, X.; Wang, P.; Ji, Y., Ultrastable aqueous phenazine flow batteries with high capacity operated at elevated temperatures. *Joule* **2021**, DOI: 10.1016/j.joule.2021.06.019.
- Wu, M.; Jing, Y.; Wong, A. A.; Fell, E. M.; Jin, S.; Tang, Z.; Gordon, R. G.; Aziz, M. J., Extremely stable anthraquinone negolytes synthesized from common precursors. *Chem* **2020**, 6, 1432–1442.
- Kwabi, D. G.; Lin, K.; Ji, Y.; Kerr, E. F.; Goulet, M.-A.; De Porcellinis, D.; Tabor, D. P.; Pollack, D. A.; Aspuru-Guzik, A.; Gordon, R. G.; Aziz, M. J., Alkaline quinone flow battery with long lifetime at pH 12. *Joule* **2018**, 2 (9), 1907–1908.
- Ji, Y.; Goulet, M.-A.; Pollack, D. A.; Kwabi, D. G.; Jin, S.; Porcellinis, D.; Kerr, E. F.; Gordon, R. G.; Aziz, M. J., A phosphonate-functionalized quinone redox flow battery at near-neutral pH with record capacity retention rate. *Adv. Energy Mater.* **2019**, 9 (12), 1900039.

12. Park, M.; Beh, E. S.; Fell, E. M.; Jing, Y.; Kerr, E. F.; De Porcellinis, D.; Goulet, M. A.; Ryu, J.; Wong, A. A.; Gordon, R. G.; Cho, J.; Aziz, M. J., A high voltage aqueous zinc-organic hybrid flow battery. *Adv. Energy Mater.* **2019**, 9 (25), 1900694.
13. Beh, E. S.; De Porcellinis, D.; Gracia, R. L.; Xia, K. T.; Gordon, R. G.; Aziz, M. J., A neutral pH aqueous organic-organometallic redox flow battery with extremely high capacity retention. *ACS Energy Lett.* **2017**, 2 (3), 639–644.
14. Jin, S.; Jing, Y.; Kwabi, D. G.; Ji, Y.; Tong, L.; De Porcellinis, D.; Goulet, M.-A.; Pollack, D. A.; Gordon, R. G.; Aziz, M. J., A water-miscible quinone flow battery with high volumetric capacity and energy density. *ACS Energy Lett.* **2019**, 4 (6), 1342–1348.
15. Gerken, J. B.; Anson, C. W.; Preger, Y.; Symons, P. G.; Genders, J. D.; Qiu, Y.; Li, W.; Root, T. W.; Stahl, S. S., Comparison of quinone-based catholytes for aqueous redox flow batteries and demonstration of long-term stability with tetrasubstituted quinones. *Adv. Energy Mater.* **2020**, 10, 2000340.
16. Tong, L.; Goulet, M.-A.; Tabor, D. P.; Kerr, E. F.; De Porcellinis, D.; Fell, E. M.; Aspuru-Guzik, A.; Gordon, R. G.; Aziz, M. J., Molecular engineering of an alkaline naphthoquinone flow battery. *ACS Energy Lett.* **2019**, 4 (8), 1880–1887.
17. Wang, C.; Li, X.; Yu, B.; Wang, Y.; Yang, Z.; Wang, H.; Lin, H.; Ma, J.; Li, G.; Jin, Z., Molecular design of fused-ring phenazine derivatives for long-cycling alkaline redox flow batteries. *ACS Energy Lett.* **2020**, 5 (2), 411–417.
18. Murali, A.; Nirmalchandar, A.; Krishnamoorthy, S.; Hooper-Burkhardt, L.; Yang, B.; Soloveichik, G.; Prakash, G. K. S.; Narayanan, S. R., Understanding and mitigating capacity fade in aqueous organic redox flow batteries. *J. Electrochem. Soc.* **2018**, 165 (7), A1193–A1203.
19. Kozlov, V. A.; Ivanov, S. N.; Koifman, O. I., Solvated proton as the main reagent and a catalyst in the single-stage aromatic sulfonation and protodesulfonation of sulfonic acids. *J. Phys. Org. Chem.* **2017**, 30 (12).
20. Xu, M.; Wan, P., Efficient photodecarboxylation of aroyl-substituted phenylacetic acids in aqueous solution: a general photochemical reaction. *Chem. Commun.* **2000**, (21), 2147–2148.
21. Samec, J. L.; Anna; Sawadjoon, Supaporn, Reduction of C–O bonds by catalytic transfer hydrogenolysis. *US 9,382,225 B2* **2016**.
22. Jing, Y.; Wu, M.; Wong, A. A.; Fell, E. M.; Jin, S.; Pollack, D. A.; Kerr, E. F.; Gordon, R. G.; Aziz, M. J., *In situ* electrosynthesis of anthraquinone electrolytes in aqueous flow batteries. *Green Chem.* **2020**, 22 (18), 6084–6092.
23. Tabor, D. P.; Gómez-Bombarelli, R.; Tong, L.; Gordon, R. G.; Aziz, M. J.; Aspuru-Guzik, A., Mapping the frontiers of quinone stability in aqueous media: implications for organic aqueous redox flow batteries. *J. Mater. Chem. A* **2019**, 7 (20), 12833–12841.
24. Hu, B.; Luo, J.; Hu, M.; Yuan, B.; Liu, T. L., A pH-neutral, metal-free aqueous organic redox flow battery employing an ammonium anthraquinone anolyte. *Angew. Chem. Int. Ed.* **2019**, 58 (46), 16629–16636.
25. Oldham, K. B.; Myland, J. C., Modelling cyclic voltammetry without digital simulation. *Electrochim. Acta* **2011**, 56 (28), 10612–10625.
26. Bourke, A.; Miller, M. A.; Lynch, R. P.; Gao, X.; Landon, J.; Wainright, J. S.; Savinell, R. F.; Buckley, D. N., Electrode kinetics of vanadium flow batteries: contrasting responses of V^{II}–V^{III} and V^{IV}–V^V to electrochemical pretreatment of carbon. *J. Electrochem. Soc.* **2015**, 163 (1), A5097–A5105.
27. Tenny, K. M.; Forner-Cuenca, A.; Chiang, Y.-M.; Brushett, F. R., Comparing physical and electrochemical properties of different weave patterns for carbon cloth electrodes in redox flow batteries. *J. Electrochem. Energy Convers. Storage* **2020**, 17 (4), 041010.
28. Yang, S.; Chen, Q., Quantifying electron transfer kinetics on porous carbon electrodes for redox flow batteries. *J. Electrochem. Soc.* **2020**, 167 (16), 160501.
29. Sedenho, G. C.; De Porcellinis, D.; Jing, Y.; Kerr, E.; Mejia-Mendoza, L. M.; Vazquez-Mayagoitia, Á.; Aspuru-Guzik, A.; Gordon, R. G.; Crespilho, F. N.; Aziz, M. J., Effect of molecular structure of

- quinones and carbon electrode surfaces on the interfacial electron transfer process. *ACS Appl. Energy Mater.* **2020**, 3 (2), 1933–1943.
30. Yang, S.; Li, Y.; Chen, Q., Resolving electron transfer kinetics in porous electrodes via diffusion-less cyclic voltammetry. *J. Mater. Chem. A* **2021**.
31. Marcus, R. A., Electron transfer reactions in chemistry: theory and experiment. *Angew. Chem. Int. Ed.* **1993**, 32, 1111–1121.
32. Lazard, Lazard's levelized cost of storage analysis — Version 5.0. **2019**.
33. Brushett, F. R.; Aziz, M. J.; Rodby, K. E., On lifetime and cost of redox-active organics for aqueous flow batteries. *ACS Energy Lett.* **2020**, 5, 879–884.
34. Kwabi, D. G.; Ji, Y.; Aziz, M. J., Electrolyte lifetime in aqueous organic redox flow batteries: A critical review. *Chem. Rev.* **2020**, 120 (14), 6467–6489.
35. Goulet, M.-A.; Aziz, M. J., Flow battery molecular reactant stability determined by symmetric cell cycling methods. *J. Electrochem. Soc.* **2018**, 165 (7), A1466–A1477.
36. Goulet, M.-A.; Tong, L.; Pollack, D. A.; Tabor, D. P.; Odom, S. A.; Aspuru-Guzik, A.; Kwan, E. E.; Gordon, R. G.; Aziz, M. J., Extending the lifetime of organic flow batteries via redox state management. *J. Am. Chem. Soc.* **2019**, 141 (20), 8014–8019.
37. Jing, Y.; Zhao, E. W.; Goulet, M.-A.; Bahari, M.; Fell, E. M.; Jin, S.; Davoodi, A.; Jónsson, E.; Wu, M.; Grey, C. P.; Gordon, R. G.; Aziz, M. J., Electrochemical regeneration of anthraquinones for lifetime extension in flow batteries. *ChemRxiv* **2021**, DOI: 10.33774/chemrxiv-2021-x05x1.
38. Pang, S.; Wang, X.; Wang, P.; Ji, Y., Biomimetic amino acid functionalized phenazine flow batteries with long lifetime at near-neutral pH. *Angew. Chem. Int. Ed.* **2021**, 60, 5289–5298.
39. Jin, S.; Fell, E. M.; Vina-Lopez, L.; Jing, Y.; Michalak, P. W.; Gordon, R. G.; Aziz, M. J., Near neutral pH redox flow battery with low permeability and long-lifetime phosphonated viologen active species. *Adv. Energy Mater.* **2020**, 10 (20), 2000100.